AIAA 80-1431R

Freestream Turbulence Effects on the Development of a Rotor Wake

C. Hah* and B. Lakshminarayana†
The Pennsylvania State University, University Park, Pa.

The effect of freestream turbulence on the development of a three-dimensional wake of a compressor rotor blade was studied experimentally. The turbulence level at the inlet of a rotor was varied systematically using grids upstream of the rotor. The rotor wake was measured with inlet turbulence intensities of 0.5, 3, and 5%. The experimental results indicate that the maximum change in the mean velocity defect is 4% over the range of inlet turbulence levels employed, while the turbulence structure in the wake is altered more substantially. The freestream turbulence effect was also analyzed, numerically, using the modified Reynolds stress closure model. The comparison between numerical prediction and experimental data shows that the freestream turbulence effect can be represented successfully with the turbulence closure model employed in this paper.

Nomenclature

C = chord length of the blade
C_l = variable in turbulence closure model, Eq. (5)
$C_s, C_{\phi l}, C_\epsilon$
$C_{\epsilon 1}, C_{\epsilon 2}, \gamma$ = constants in turbulence closure models
g_{ij} = fundamental metric tensor, Eq. (2)
L = integral length scale, TU
P = $-\overline{u_i u_j} U^i_{,j}$
p = static pressure
p^* = reduced static pressure
Q = total mean velocity
Re = Reynolds number based on chord length
S = blade spacing in rotor
s,n,r = curvilinear coordinate system; $s=0$ at the trailing edge, $n=0$ at the wake center
T = integral scale in Table 1 $\left[\int_0^\infty \rho(\tau)\,d\tau\right]$
U^i, u^i = contravariant mean and fluctuating velocity components [U,V,W,u,v,w in (s,n,r) coordinates]
$\overline{u^i u^j}$ = Reynolds stress components
$\overline{-vw}/U^2$ = radial-shear stress
$\overline{-uv}/U^2$ = streamwise-shear stress
u^* = friction velocity
β = angle between machine axis and streamwise direction
δ = boundary-layer thickness
δ^* = displacement thickness
ϵ^{ijk} = permutation tensor
θ = momentum thickness
κ = turbulence kinetic energy
ν = kinetic viscosity
ρ = density
$\rho(\tau)$ = autocorrelation coefficient $[\overline{u(t)u(t-\tau)}/\overline{u^2}]$
Γ^i_{jk} = Christoffel symbol of second kind
τ = time delay in autocorrelation
Ω_j = angular velocity of rotor

Subscripts

∞ = values in the freestream
c = values of wake center
t = values at the tip
m = maximum values

Superscript

$\bar{()}$ = average value

Introduction

TO predict the development of boundary layers on the turbomachinery blades and resulting turbulent wakes behind the blades accurately, the external freestream conditions should be properly included in the numerical scheme. The turbulence level at the inlet of the turbomachinery may be very low (less than 0.5%). However, the turbulence level may reach high values (10%) after a few stages (rows of blades) in a multistage compressor or a turbine. Although many investigators have argued that the differences between the performance of compressors and the respective cascades are due to the different turbulence levels, the effects of freestream turbulence have not been explored satisfactorily in a full-scale turbomachinery rotor.

Few experimental studies have been reported on the freestream turbulence effects on the development of turbulent boundary layers even for simple configurations. Kline et al.[1] investigated the effects of increasing the freestream turbulence level on the boundary-layer growth. They noticed an increase in boundary-layer thickness δ, and in skin friction C_f, with an increasing freestream turbulence level. These effects were also observed by Robertson and Holt.[2] Huffman et al.[3] carried out a detailed study of the structural properties of the turbulent boundary layer developing under various levels of freestream turbulence. They found an increase in the turbulence intensities, turbulent kinetic energy, and Reynolds shear stress at the outer edge of the boundary layer as the freestream turbulence level was increased. Evans[4] took detailed measurements of the mean velocity as well as the turbulence quantities in a constant-pressure turbulent boundary layer under various freestream turbulence levels. His studies showed an increase in skin friction and the velocity gradient near the solid wall with high freestream turbulence level. He also observed an increase in the turbulent kinetic energy and Reynolds shear stress throughout the boundary layer.

The freestream turbulence effects on the flow around a cascade of airfoils have been studied primarily for the overall performance of the cascade. Hebbel[5] found that high freestream turbulence decreases the overall loss for a certain range of Reynolds number and increases the overall loss

Presented as Paper 80-1431 at the AIAA 13th Fluid and Plasma Dynamics Conference, Snowmass, Colo., July 14-16, 1980; submitted Aug. 14, 1980; revision received Jan. 28, 1981.

*Research Associate in Aerospace Engineering, Department of Aerospace Engineering. Member AIAA.

†Director of Computational Fluid Dynamics Studies and Professor of Aerospace Engineering, Department of Aerospace Engineering. Associate Fellow AIAA.

beyond a certain Reynolds number. Kiock[6] observed a critical degree of turbulence, at which the transition moves suddenly upstream of the blade by a substantial amount and the flowfield does not change further even if the turbulence level is increased thereafter. Schlichting and Das[7] argued that the vigorous diffusion due to the turbulence in the flowfield delays separation of the boundary layer and consequently reduces the overall drag.

For the effects of freestream turbulence in an actual compressor or a turbine, Kiock[8] measured passage-average turbulence intensity, but no detailed measurements of turbulence and its effects have been reported.

When the freestream turbulence level is increased, energy-containing eddies in the freestream interact with the flow inside the boundary layer, promote earlier transition to turbulence, and delay or prevent the flow separation. Downstream of the blade, the viscous region is considered to penetrate more rapidly to the freestream due to higher freestream turbulence level.

The effects of freestream turbulence on the boundary-layer development of the blade depends on the critical degree of the turbulence, which is a function of Reynolds number, shape of the blade, pressure distribution, and possibly rotation. When the freestream turbulence level varies beyond the critical degree of turbulence, the effects of freestream turbulence are small; however, these effects become substantial when the turbulence level varies below the critical degree.

A knowledge of the effects of in-flow turbulence on the rotor wake is of great significance in evaluating the various sources of fan noise. Recent investigations (e.g., Refs. 9 and 10) suggest that in-flow control devices such as honeycomb and grid bring about a substantial reduction in the tonal intensity at the blade passing frequency (BPF). Without such a control, the long eddies resulting from the contraction of the inflow eddies in a static facility generate high BPF noise. It has been postulated that the long eddies present in a static facility is not typical of those that exist during flight. Some doubts have been expressed as to whether the reduction in noise with inflow control is brought about by the reduction in length scale or by the alteration of the characteristics of the rotor wake, which is also responsible for BPF noise. One of the major objectives of this paper is to study the effect of in-flow turbulent structure (length scale and intensity) on the rotor wake characteristics.

In a work reported here, the effects of the freestream turbulence level on the development of the rotor wake were studied experimentally by varying the inlet turbulence level systematically with different grids. The effects were also studied numerically and the results are compared with the experimental data.

Theoretical Considerations

A curvilinear coordinate system (s,n,r) was used for the wake prediction, with an approximate streamwise direction s on the cylindrical surface, principal normal n being perpendicular to this streamline on the cylindrical surface. The radial direction was the third coordinate. The detailed characteristics of this coordinate system are given by Hah and Lakshminarayana.[11] The governing equations are as follows in generalized tensor form for incompressible flow.

Continuity:

$$U^i_{;j}=0, \quad u^i_{;j}=0 \tag{1}$$

Momentum Conservation:

$$U^j U^i_{;j}+\overline{u^j u^i_{;j}}+2\epsilon^{ijk}\Omega_j U_k=-\frac{g^{ij}}{\rho}\frac{\partial P^*}{\partial x^j}+\nu g_{jk}U^i_{;jk} \tag{2}$$

where P^* is the reduced pressure ($P^*=P-\rho\Omega^2 r^2/2$) and all other terms are given in the Nomenclature.

For the closure of the governing equations, modified Reynolds stress closure is used. The diffusion and the convection terms in the Reynolds stress transport equations are considered collectively and the combined effect of the two terms are assumed to be related to the production term. A variable, whose values are evaluated using the upstream flow condition and updated during the iteration, is introduced to represent the collective effects of the two terms. Also rotation-originated redistribution terms are added in the Reynolds stress transport equation. With the previous assumption, six components of Reynolds stress can be calculated with the modeled Reynolds stress equation if the mean shear rate, turbulence kinetic energy, and the energy dissipation rate are given at each grid point in the flowfield. The following transport equations for the turbulence kinetic energy, energy dissipation rate, and Reynolds stress are used:

$$U^k\frac{\partial \epsilon}{\partial x^k}=S-C_{\epsilon_2}\frac{\epsilon^2}{\kappa}+C_\epsilon\left(\frac{\kappa}{\epsilon}\overline{u^k u^l}\frac{\partial \epsilon}{\partial x^l}\right)_{,k} \tag{3}$$

$$U^k\frac{\partial \kappa}{\partial x^k}=p-\epsilon+C_s\left(\frac{\kappa}{\epsilon}\overline{u^k u^l}\frac{\partial \kappa}{\partial x^l}\right)_{,k} \tag{4}$$

and

$$0=(1+C_1)(-\overline{u_k u^j}U^i_{,k}-\overline{u_k u^i}U^j_{,k})(1-\gamma)-2(\epsilon^{ilm}\Omega_l\overline{u_m u^j}$$

$$+\epsilon^{jlm}\Omega_l\overline{u_m u^i})-\tfrac{2}{3}g^{ij}\epsilon(1-\gamma)-C_{\phi_1}\frac{\epsilon}{\kappa}(\overline{u^i u^j}-\tfrac{2}{3}g^{ij}\kappa) \tag{5}$$

where $\kappa=\frac{1}{2}g_{ij}\overline{u^i u^j}$, ϵ is the rate of energy dissipation, $p=-u_i u_j U^i_{,j}$, $S=(C_1\epsilon^2/\kappa^2)(\overline{u^i u^j}-\frac{2}{3}\kappa\delta_{ij})(\overline{u^j u^i}-\frac{2}{3}\kappa\delta_{ji})$; γ, C_{ϕ_1}, C_{ϵ_2}, C_ϵ, C_s, and C_1 are constants. C_1 is variable, and represents the collective effects of the convection and the diffusion terms in the transport equation of Reynolds stresses.

The numerical values for the universal constants were not optimized for the present study even though a slightly higher value of C_{ϵ_1} resulted in a better prediction. The numerical values used are $C_s=1$, $C_1=1.8$, $C_\epsilon=0.15$, $C_{\epsilon_1}=1.45$, $C_{\epsilon_2}=1.9$, and $\gamma=0.6$.

As the present turbulence closure model solves the turbulence kinetic energy κ, the rate of energy dissipation ϵ, and the Reynolds stress components, the freestream turbulence level can be specified in the numerical scheme through the boundary condition. For elliptic calculation, boundary conditions were specified on the whole boundary surfaces. These boundary conditions were based on the experimental data and the correlation of the experimental data. Details of the numerical scheme, step size, and accuracy are given in Ref. 11.

Experimental Facility, Procedure, and Program

Facility and Procedure

The experiments reported in this paper were conducted in a single-stage axial flow compressor. The general description of the stage and the operating characteristics are given by Lakshminarayana.[12] The rotor, with 21 cambered and twisted blades, was housed between an inlet guide vane assembly and a stator assembly. The rotor tip radius was 0.4661 m with a hub-to-tip ratio of 0.5. The blade element data at midradius are modified NACA 65-010 basic profile with a circular arc camber, chord 0.134 m, maximum thickness 6.65% of chord, stagger angle 30 deg. All experiments were done at the operating flow coefficient of 0.56 (based on the blade tip speed). All measurements in the rotor wake were conducted behind the rotor at a radius (midspan) of 0.35 m ($r/r_t=0.7297$) and at various axial locations. The rotor was operated at 1066 rpm with an inlet (to the guide vane) axial velocity of 30.5 m/s.

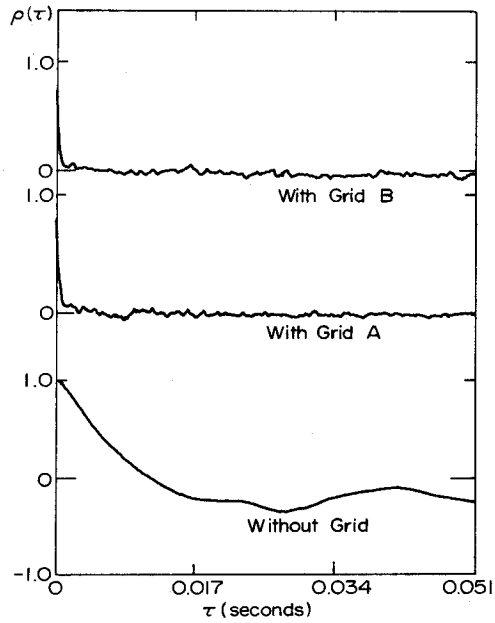

Fig. 1 Autocorrelation at inlet of the rotor.

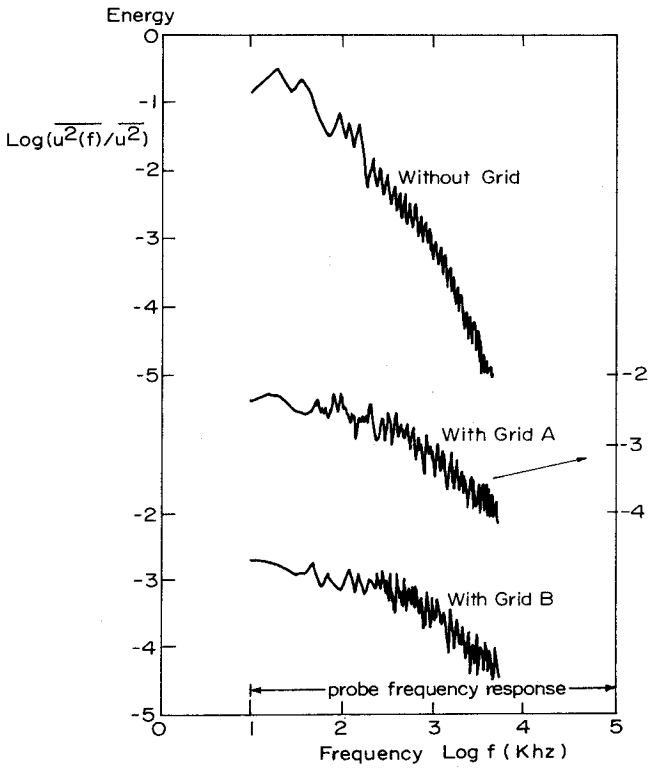

Fig. 2 Energy spectrum at inlet of the rotor.

Two different grids were located before the inlet guide vane of the compressor to increase the freestream turbulence level. The grids were composed of square sections made with cylindrical bars. Grid A consisted of 4.76 mm bars spaced at 25.4 mm apart. Grid B was of similar construction with a spacing of 12.7 mm. The flow characteristics at inlet freestream were measured at midradius and 0.17 chord length upstream of the rotor blade. The freestream turbulence level was 0.5% at the inlet of the rotor when no grid was used, and the measured relative turbulence intensities were 3 and 5%, respectively, with grids A and B. The autocorrelation and the energy spectra at the inlet of the rotor blade are shown in Figs. 1 and 2, respectively.

The inlet flow has large eddies when the grids were not used, as shown in Fig. 1, and these large eddies are chopped into smaller eddies by the grids. The measured spectra in the freestream show that the energy is considerably increased in the high-frequency range when the grids are used with a consequent increase in the freestream turbulence level.

Table 1 Turbulence characteristics at inlet to the rotor

	$\sqrt{u^2}/U_\infty$, %	T, s	L, cm	Slope in spectrum
No grids	0.5	0.00725	22	−5/3
Grid A	3.0	0.00119	3	−1
Grid B	5.0	0.00102	2	−1

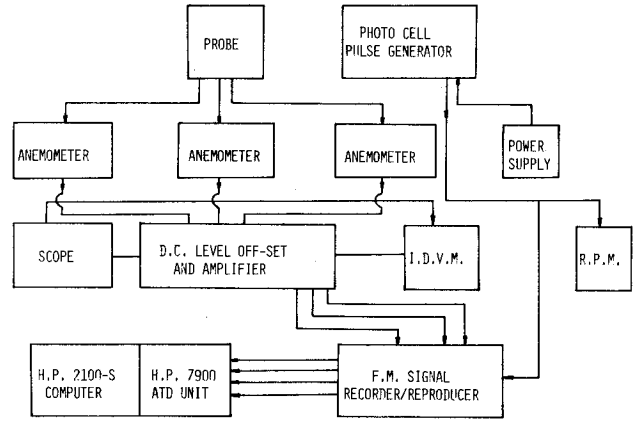

Fig. 3 Block diagram of instrumentation.

The turbulence intensity, integral time scale, length scale, and the slope of spectrum are given in Table 1. The integral time scale was obtained from the plot of autocorrelation coefficient (Fig. 1) using the following relationship:

$$T = \int_0^\infty \rho(\tau)\,d\tau$$

The integral length scale was obtained by multiplying the integral time scale with the local mean velocity.

When no grid was used, the slope in the energy spectrum at higher frequency (Fig. 2) has value of −5/3. This is due to a relatively high Reynolds number and the isotropic nature of turbulence. When grids are used to increase the turbulence intensity, decreased length scales cause a change in the spectrum as shown in Fig. 2. The observed slope is −1 in this case. Also more kinetic energy is transferred to the eddies of middle frequency range when grids are used.

A miniaturized triaxial hot-wire probe manufactured by DISA was used for the measurements of mean velocity and turbulence quantities in the rotor wake. The length of each hot wire in the probe was approximately 0.009 m with the diameter of 3 μm and the resistances were 4.02, 4.12, and 4.25 Ω. The three hot wires were located inside a sphere whose diameter was 0.0018 m. The probes were located in the wake so as to place the measuring velocity vector inside the inner cone formed by the three sensors. The sensors were connected to three DISA 55M10 constant-temperature anemometers. A frequency gain of 4 was set for the anemometers and the frequency response of the sensor was from 16 to 10^5 Hz. The maximum frequency of the flowfield corresponding to Kolmogorov scale is about 5 kHz and the frequency of the probe is well above that of the actual flowfield. The signals from these three anemometers were fed to an integral digital voltmeter to get the overall mean voltage of the anemometer output. Also, the fluctuating ac signals were amplified and recorded in an FM signal recorder/reproducer. The signals were then digitized and processed statistically in a Hewelett Packard 2100 S computer system. The block diagram of instrumentation is given in Fig. 3.

Data Processing

As the present experiments adopt a stationary triaxial probe, the hot wires sense the random fluctuation as well as the periodic variation of velocity vector in the wakes of 21 rotor blades. The random fluctuation as well as the periodic variation of velocity vector should be properly separated during the data processing so that mean velocity and turbulence quantities across the wake can be derived from the data. To identify the specific wake from 21 consecutive wakes of rotor blades in data processing, a pulse generator was installed in the compressor axis. This pulse generator provides one sharp pulse per each revolution of the compressor axis when the specified blade passes a certain reference point. With this pulse signal, all of the wakes, as well as the relative position of the rotor blades to the probe, can be identified. The ensemble-average technique was used to obtain the mean velocity and the turbulence quantities across the wake. Since the rotational speed of the compressor rotor is high (for the present experiment without grid, 1066 rpm), one wake passage takes very little time (for the present case, 0.0027 s). To extract important information from the experimental data, many measuring points are necessary in one wake passage. Three-hundred sampling points per wake were used in the present experiment. If the data is to be processed at real time, the analog signal should be digitized at an impractically high sampling speed (2.5 μs sampling interval). Therefore, the analog signal was digitized at 1/16 real time (40 μs of the sampling interval). With the pulse signal, only the wakes of the specific blade were continuously digitized. The digitized hot-wire signal was converted to the corresponding instantaneous cooling velocity. Instantaneous flow velocity was obtained from the cooling velocities of three wires using hot-wire equations, and various mean and turbulence flow characteristics were obtained through the ensemble average. The hot-wire equations and statistical procedure utilized are given in Ref. 13.

Experimental Results

Transition

To find out any change of transition zone on the blade surface due to the freestream turbulence level, the flowfield on the blade surface near the leading edge was visualized. The china clay technique, previously used for the visualization of the flow on the helical blade by Lakshminarayana et al.[14] was utilized. The mixture of china clay, water, acetone, and glycerol was sprayed over the blade surface to get a white film of china clay over the blade surface. When a chemical liquid of the same index of retraction is sprayed over the film, the film becomes transparent, but a white deposit reappears as soon as the evaporation is completed. The evaporation takes place faster in the turbulent region than in the laminar region, as indicated by the whiteness of the former and the darkness of the latter regions. As was expected at high Reynolds number ($Re = 4.6 \times 10^5$), the transition does occur at the very leading edge of the blade for all three freestream turbulence levels. Compared to the critical degree of turbulence for the cascade, which is 2.5% at $Re = 1.6 \times 10^5$ (Ref. 6), the effect of rotation and three-dimensional character of the flowfield may further decrease the turbulence level required for the early transition. This may be the reason why the transition happens at an early stage even for the lowest freestream turbulence level tested. Therefore, any effects on the flowfield due to the laminar bubble near the leading edge of the blade are not considered for the present experiment.

Mean Velocity

Figure 4 shows the streamwise and radial mean velocity profiles in the rotor wake at different freestream turbulence levels. The change in streamwise velocity profile is appreciably smaller than expected. As can be seen in the figure, the wake region penetrates further into the freestream when the freestream turbulence level is increased. This is due to intense turbulent mixing in the outer layer of the wake by energy-containing eddies in the freestream. Also, there is an appreciable change in the velocity profile, especially in the outer layer, when the freestream turbulence level is increased. Both the streamwise and radial mean velocity profiles show that the velocity gradient in the wake center becomes steeper and the velocity gradient in the outer layer becomes more gradual when the freestream turbulence level is increased. This is caused when turbulent mixing in the outer layer is increased resulting in a smaller velocity gradient in that region. Earlier transition to turbulent flow in the boundary layer on the blade due to a high freestream turbulence level also causes this phenomenon, because of high diffusion in the turbulent flow. This was observed by Evans[4] in the turbulent boundary layer developing under different freestream turbulence levels. The radial mean velocity profiles of the rotor wake show inward and outward flow near the trailing edge region. The radial velocities are outward away from the trailing-edge region. The radial velocity decreases in the outer layer as the freestream turbulence level is increased.

Figure 5 shows the downstream variation of displacement and momentum thickness for the different freestream turbulence levels. The displacement thickness δ^* and momentum thickness θ are defined as

$$\delta^* = \frac{1}{S}\int_0^S \left(1 - \frac{Q}{Q_\infty}\right) dn \tag{6}$$

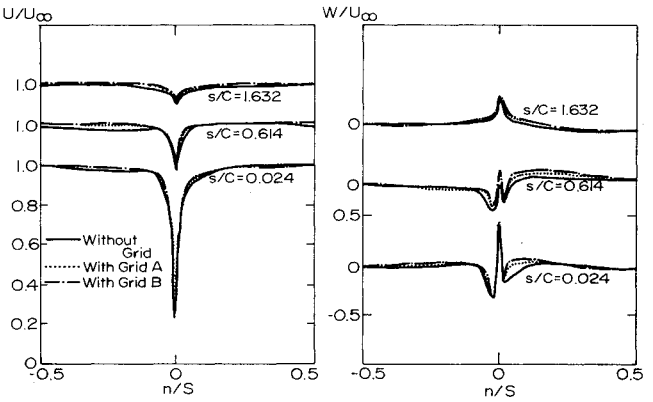

Fig. 4 Streamwise and radial mean velocity profiles in the wake.

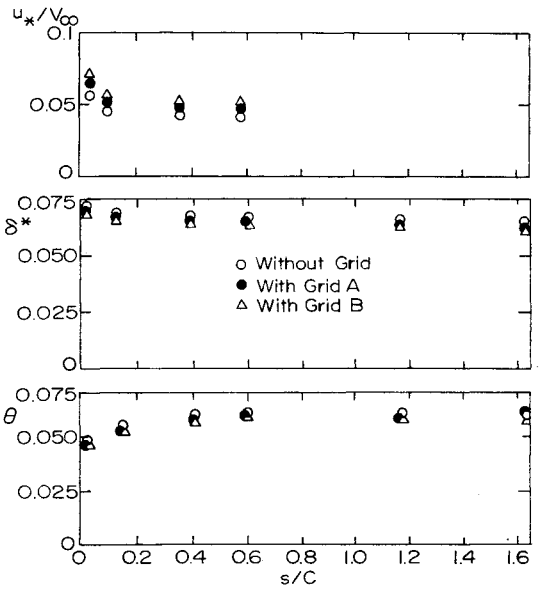

Fig. 5 Downstream variation of displacement thickness, momentum thickness, and friction velocity.

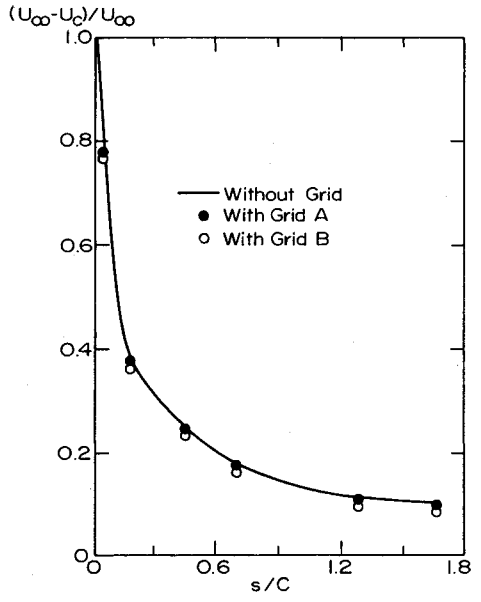

Fig. 6 Decay of streamwise mean velocity defect.

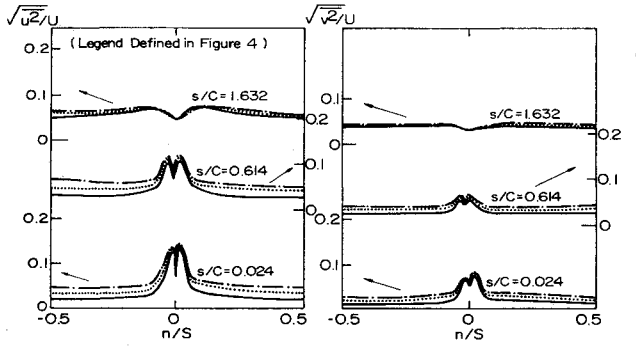

Fig. 7 Distribution of streamwise and normal turbulence intensities.

$$\theta = \frac{1}{S}\int_0^S \left(1-\frac{Q}{Q_\infty}\right)\frac{Q}{Q_\infty}\,dn \qquad (7)$$

where Q_∞ is the total mean velocity at the freestream. As seen in Fig. 5, the displacement and the momentum thicknesses decrease slightly when the freestream turbulence level is increased. This can be explained as follows. The vigorous interaction between the wake and freestream make the wake wider and consequently change the displacement and the momentum thicknesses. The change in the velocity profile towards a steeper profile near the wake center tends to decrease these thicknesses. At the three streamwise stations nearest to the blade trailing edge, the streamwise friction velocity was calculated with the assumption that the logarithmic velocity profile is conserved at the wake center region. The calculated friction velocities for three freestream turbulence levels are also shown in Fig. 5 and indicate that the friction velocity increases slightly with the increase in freestream turbulence.

Figure 6 shows the decay of the streamwise mean velocity defect at the wake center at three freestream turbulence levels. The mean velocity defect decays slightly faster with the increase in the freestream turbulence level. If the variation of wake centerline velocity in the very near wake is assumed to be governed by the surrounding viscous sublayer, as measurements for the isolated airfoil wake suggest, the wake centerline velocity in the near wake can be represented as follows[13] by solving the streamwise momentum equation on the wake centerline:

$$\frac{U_c}{u^*} = \sqrt{\frac{2}{5}\left(\frac{u^* s}{\nu} - \frac{5}{\rho}\frac{\partial p}{\partial s}\frac{s}{u^{*2}}\right)} + F(\Omega) \qquad (8)$$

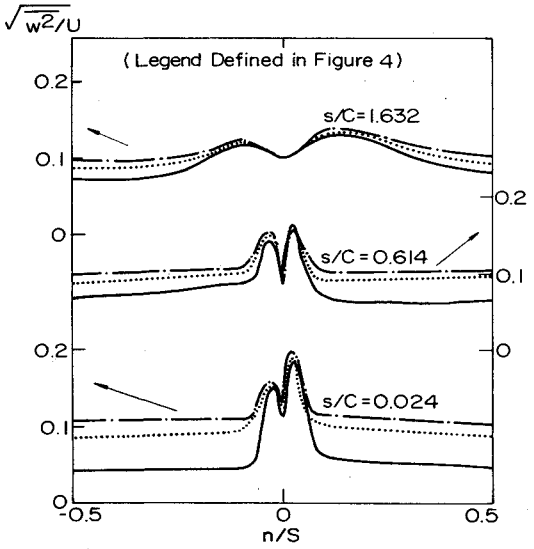

Fig. 8 Distribution of radial turbulence intensity.

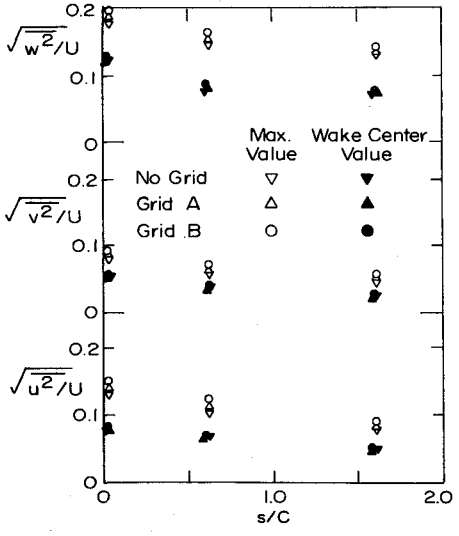

Fig. 9 Variation of maximum turbulence intensity and wake centerline turbulence intensity.

where s is distance from the trailing edge on the wake centerline, U_c the wake centerline velocity (U_c is zero at trailing edge), and $F(\Omega)$ represents the effects of rotation. As was shown in Fig. 5, the friction velocity is higher when the freestream turbulence level is increased. Therefore, the decay of the wake centerline velocity defect is faster [Eq. (8)] for the same pressure gradient.

Turbulence Quantities

Figures 7 and 8 show the distribution of turbulence intensity across the wake at several streamwise locations at different freestream turbulence levels. There is a slight increase in turbulence intensity in the wake center region, but a marked increase in the outer layer. The ratio of maximum intensity at the wake centerline to the freestream turbulence intensity decreases with the increase in freestream turbulence level. This seems to indicate that freestream turbulence has relatively little influence on the turbulence levels at the wake center. The ratio of the radial-turbulence intensity to the streamwise-turbulence intensity increases due to the effect of rotation in a rotor wake. This is found to be true at all the freestream turbulence levels. Figure 9 shows the downstream variation of the maximum turbulence intensity and the wake centerline turbulence intensity at different freestream turbulence levels. The maximum turbulence intensity increases

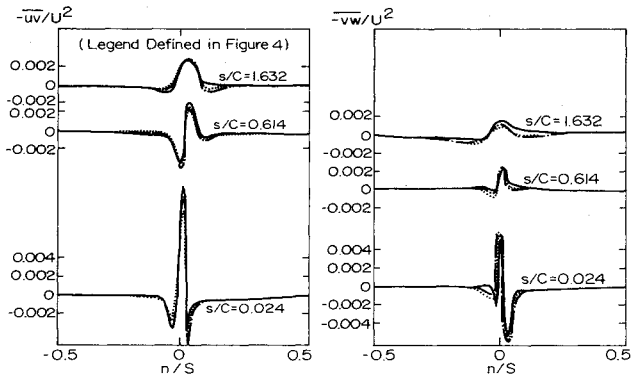

Fig. 10 Distribution of Reynolds shear stresses.

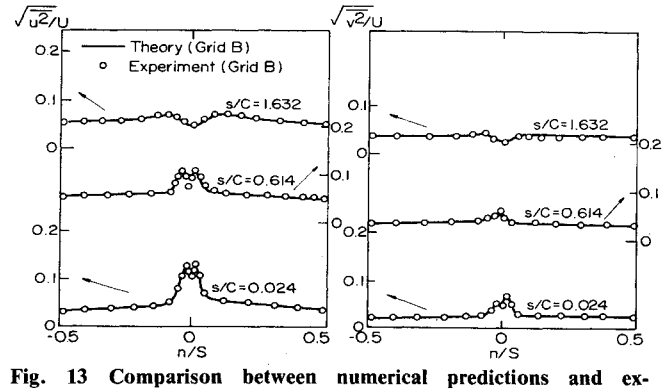

Fig. 13 Comparison between numerical predictions and experimental data of streamwise and normal turbulence intensity profiles.

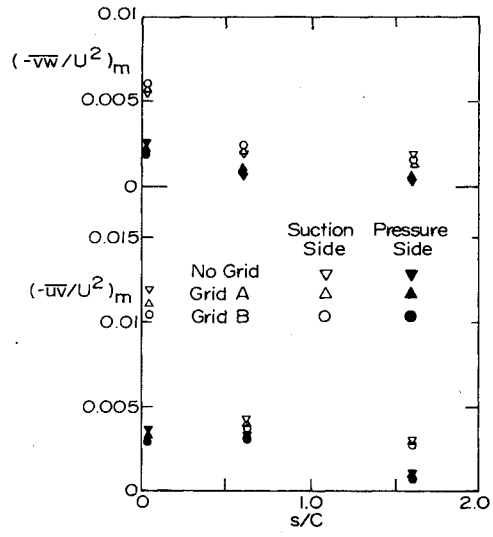

Fig. 11 Variation of maximum Reynolds shear stress in the suction side and in the pressure side of the wake.

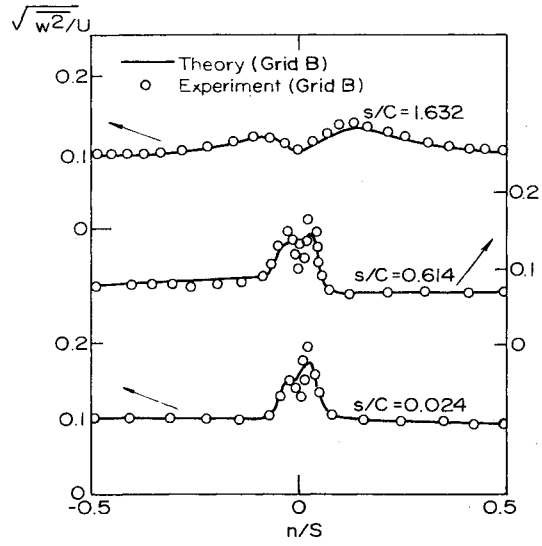

Fig. 14 Comparison between numerical predictions and experimental data of radial turbulence intensity profile.

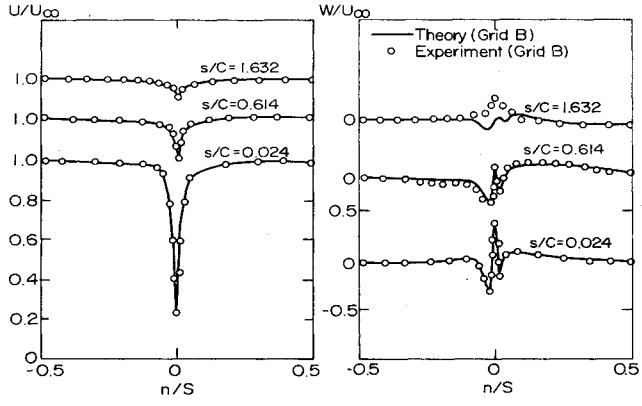

Fig. 12 Comparison between numerical predictions and experimental data of mean velocity profile.

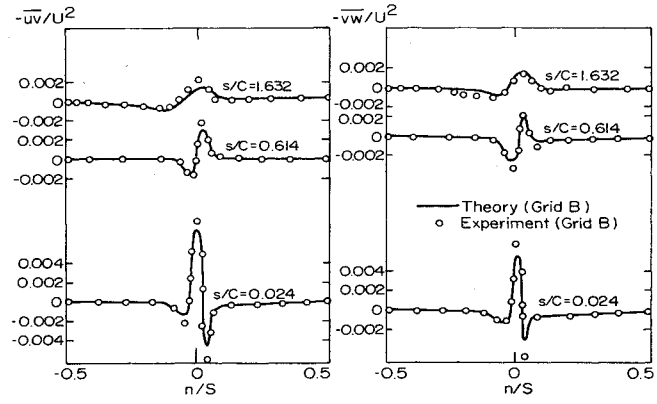

Fig. 15 Comparison between numerical predictions and experimental data of Reynolds shear stress profile.

with an increase in the freestream turbulence level, but decays faster at higher values of freestream turbulence intensity. The ratio of maximum radial-turbulence intensity to the maximum streamwise-turbulence intensity decreases with an increase in the freestream turbulence level. It is evident from these measurements that the turbulence intensity at wake centerline does not change with the freestream turbulence level. Major effects are confined to outer regions of the wake, with little or no change at the wake center.

In Fig. 10, the distribution of Reynolds shear stress across the wake is shown for three freestream turbulence levels. There seems to be a slight increase in the radial shear stress component and a slight decrease in the streamwise shear stress component with a high level of freestream turbulence. Also, the shear stress is observed to persist further into the freestream when the freestream turbulence level is increased. The downstream variation of the maximum shear stress is shown in Fig. 11 at different freestream turbulence levels. The

maximum streamwise shear stress decreases at higher freestream turbulence level while the maximum radial-shear stress increases. The ratio of the maximum streamwise-shear stress to the maximum radial-shear stress decreases with an increase in freestream turbulence level.

Comparison of the Experimental Data with the Numerical Predictions

The development of the rotor wakes under high freestream turbulence levels was also predicted, numerically, using a modified Reynolds stress model, Eqs. (3-5). The effect of rotation is represented through the rotation-originated redistribution term in the modeled Reynolds stress transport equation. The detailed description of the turbulence closure model and numerical technique for the low freestream turbulence level are given by Hah and Lakshminarayana.[11] The high freestream turbulence level is incorporated in the numerical scheme through the boundary condition in the freestream. The turbulence kinetic energy in the freestream was based on the relative turbulence intensity (3 and 5% with grids). The rate of turbulence kinetic energy dissipation on the boundary was assumed to be equal to the energy production. The effective eddy viscosity is approximately proportional to κ^{2}/ϵ in the present turbulence closure model, and a higher value of κ in the freestream means more active turbulent diffusion in the outer region of the wake.

Comparison of the data without any grid and the prediction are discussed in Ref. 11. In Fig. 12, the numerical predictions of the mean velocity profiles are shown compared with the experimental data with grid B (5% freestream turbulence intensity). Although there exists some deviation between the prediction and the experimental data, the agreement is excellent if the complexity of the flowfield is considered. Also, the faster decay of wake velocity defect under a high freestream turbulence level is properly predicted. Figures 13-15 show the comparison of turbulence properties. Even though deviations between the experimental data and the predictions are observed, the general trend of the effects due to a high freestream turbulence level is predicted properly with the utilized turbulence closure model and the numerical scheme. This seems to indicate that the turbulence model and the numerical scheme employed in this and earlier investigation[9] can simulate adequately the effects of freestream turbulence.

Conclusions

The effect of the freestream turbulence level on the development of the rotor wake was studied both experimentally and analytically. The flow visualization for the transition zone showed that the transition occurs the leading edge of the blade for the freestream turbulence intensities of 0.5, 3, and 5%, respectively. This is due to the relatively high Reynolds number. Experimentally observed effects of high freestream turbulence level are as follows:

1) The effect of the presence of grids upstream of the rotor is to increase the freestream turbulence level and decrease the length scale of turbulent eddies. However, there is no appreciable change in the overall characteristics of the rotor wake. This indicates that the decrease in the turbulence length scales may be more responsible for the reduction of BPF noise observed by many investigators.

2) A steeper velocity gradient in the wake center and consequent higher friction velocity is observed.

3) A slightly faster decay of the wake velocity defect is observed.

4) An increase in turbulence intensity and turbulent kinetic energy, especially in the outer layer of the wake where the wake interacts with the freestream, is measured.

5) An increase in the radial Reynolds shear stress component and a penetration of the shear stress into the freestream is measured.

6) The development of the rotor wake was also numerically predicted with a modified turbulence closure model. The high freestream turbulence level was incorporated through the boundary condition into the numerical scheme. The comparison between the predictions and the experimental data indicates that the effect of the freestream turbulence level is well represented in the numerical analysis and turbulence models employed in this investigation.

Acknowledgments

This work was supported by NASA through Grant NSG 3012, with Loretta Shaw as the technical monitor.

References

[1] Kline, S. J., Lisin, A. V., and Waitman, B. A., "Preliminary Experimental Investigation of Effects of Free-Stream Turbulence on Turbulent Boundary Layer Growth," NASA TN D-368, 1960.

[2] Robertson, M. J. and Holt, D. F., "Free-Stream Turbulence Effects on the Turbulent Boundary Layer," *Proceedings of ASCE*, Vol. 98, June 1972.

[3] Huffman, G. D., Zimmerman, D. R., and Bennet, W. A., "The Effects of Free Stream Turbulence Level on Turbulent Boundary Layer Behavior," AGARD-AG-164, 1972, pp. 91-116.

[4] Evans, R. L., "Free Stream Turbulence Effects on the Turbulent Boundary Layer," ARC C.P. No. 1282, June 1973.

[5] Hebbel, H. H., "Uber den Einfluss der Machzahl und der Reynoldszahl auf die Aerodynamischen Beiwerte von Verdichter-Schaufelgitten bei verschiedener Turbulenz der Stromung," *Forschgung in Ingenieuswesen*, Vol. 33, No. 5, 1967, pp. 141-150.

[6] Kiock, R., "Influence of the Degree of Turbulence on the Aerodynamic Coefficients of Cascades," *Boundary Layer Effects in Turbomachines*, AGARDograph 164, 1972, pp. 73-88.

[7] Schlichting, H. and Das, A., "On the Influence of Turbulence Level on the Aerodynamic Losses of Axial Turbomachines," *Flow Research on Blading*, edited by L. S. Dzung, Elsevier Publishing Co., 1970.

[8] Kiock, R., "Turbulence Downstream of Stationary and Rotating Cascades," ASME Paper 73-GT-80, 1973.

[9] McArdle, J. C. et al., "Comparison of Several Inflow Control Devices for Flight Simulation of Fan Noise Using a JT15D-1 Engine," AIAA Paper 80-1025, 1980.

[10] Moiseev, N., Lakshminarayana, B., and Thompson, D. E., "Noise Due to Interaction of Boundary Layer Turbulence with a Compressor or Propulsor Rotor," *Journal of Aircraft*, Vol. 15, Jan. 1978, pp. 53-61.

[11] Hah, C. and Lakshminarayana, B., "Numerical Analysis of Turbulent Wakes of Turbomachinery Rotor Blades," *Journal of Fluids Engineering*, Vol. 102, Dec. 1980, pp. 462-471.

[12] Lakshminarayana, B., "An Axial Flow Research Compressor Facility Designed for Flow Measurement in Rotor Passage," *Journal of Fluids Engineering*, Vol. 102, Dec. 1980, pp. 402-411.

[13] Hah, C., "A Numerical and Experimental Study of the Turbulent Wakes of Turbomachinery Rotor Blades, Isolated Airfoils, and a Cascade of Airfoils," Ph.D. Thesis, The Pennsylvania State University, March 1980.

[14] Lakshminarayana, B., Jabbari, A., and Yamaoka, H., "Turbulent Boundary Layer on a Rotating Helical Blade," *Journal of Fluid Mechanics*, Vol. 51, Feb. 1972, pp. 554-569.